arXiv:0904.0176v1 [cond-mat.mtrl-sci] 1 Apr 2009

Modeling self-assembly of diblock copolymer-nanoparticle composites

Fábio D. A. Aarão Reis*

Department of Chemistry, University of Wisconsin - Madison, Wisconsin 53706, USA

(Dated: April 1, 2009)

Abstract

A cell dynamics method for domain separation of diblock copolymers (DBCPs) interacting with nanoparticles (NPs) whose diffusion coefficients depend on chain configuration is proposed for self-assembly of DBCP/NP composites. Increasing NP concentration slows down domain separation, but matching NP diffusion lengths and lamellar size of DBCPs reduces this effect. The model also explains features of different nanocomposites, such as morphological transitions induced by NPs, the coexistence of lamellar and hexagonal patterns in a single sample and peaked NP density profiles across the parallel domains.

* On leave from Universidade Federal Fluminense (Brazil). Email addresses: fdreis@wisc.edu, reis@if.uff.br.

I. INTRODUCTION

Mixtures of diblock copolymers (DBCPs) and nanoparticles (NPs) have attracted much interest in recent years [1, 2]. The microphase separation of the DBCPs is expected to template NP arrangement, which may improve the physical properties of the composite or facilitate the production of other nanostructures of technological interest. However, the interaction of DBCPs and NPs may lead to a nontrivial morphology even with low NP loadings [3, 4, 5, 6, 7], as anticipated by models of mixtures in thermodynamic equilibrium [8, 9]. This motivated intense theoretical work [10], usually focusing on equilibrium properties. However, the most highly ordered patterns are obtained in far from equilibrium conditions [11] and typical self-assemble times are of several hours or days. Thus, understanding the pathways to form the desired structures is essential to improve production methods.

This paper introduces a model for self-assembly of a mixture of DBCPs and ex-situ formed NPs that describes features of various real composites. A cell dynamics method (CDM) [12, 13] represents the main physico-chemical mechanisms of domain separation of DBCPs and provides a realistic nanopattern morphology. The CDM variables, which represent the local chain configurations, interact with NPs whose diffusion coefficients depend on those configurations. Our CDM/NP model resembles those of Refs. [14, 15], but it is a significant extension of them because it accounts for a wider range of polymer-particle interactions. Compared to other recent models, the advantage of the CDM/NP approach is to address non-equilibrium and steady state features simultaneously.

Among the non-equilibrium features represented by our model, emphasis is given to the role of particle mobility on the slow down of microphase separation and the effects of NP concentration. High NP mobility is shown to destroy phase separation, while very low mobility delays the alignment with an interacting surface by freezing internal domain configurations. Connections with experimental work [16, 17] are discussed and acceleration of global ordering is suggested to occur when the NP diffusion lengths at the pure DBCP ordering time matches the lamellar size. The model also explains equilibrium features observed in experiments, such as the peaked or broad distributions of NP positions across DBCP lamellae [18, 19], the morphological transitions induced by NP loading [17, 20, 21, 22], and the coexistence of different domain patterns in a single sample interacting with a surface [5, 23].

The rest of this work is organized as follows. In Sec. II, we present the model and

discuss the simulation procedure. In Sec. III, we discuss the non-equilibrium evolution of the DBCP/NP composites, with a focus on the case in which the mixture interacts with an aligning surface. In Sec. IV, we show how the increase of NP concentration may change the morphology of the composites, in some cases producing samples where different structures coexist. In Sec. V, we show the relation of NP diffusion coefficients and the distribution of NPs across the ordered domains. In Sec. VI we summarize our results and conclusions.

II. MODEL AND SIMULATION PROCEDURE

In the CDM, a field variable $\psi(\vec{r},t)$ at cell $\vec{r}$ represents the state of a nanoscopic region of a DBCP sample at time t. The cell size is the length unit of the model and this is also the particle size, as discussed below, thus it is expected to correspond to lengths between $2nm$ and $10nm$ in most applications (may be slightly larger in some cases). We will work with lamellar sizes which are typically ten times larger than the cell sizes, which in most cases correspond to high molecular weight polymers.

In a unit time interval, ψ evolves as

$$\psi(\vec{r},t+1) = \langle\langle\psi(\vec{r},t)\rangle\rangle + \Gamma(\vec{r},t) - \langle\langle\Gamma(\vec{r},t)\rangle\rangle - B\psi(\vec{r},t) + \xi(\vec{r},t), \tag{1}$$

where Γ contains short-range interaction terms, $-B\psi(\vec{r},t)$ accounts for long-range interactions that restrict domain coarsening to a nanoscopic lengthscale, and ξ is a thermal (conservative) noise. $\tilde{\Delta}X \equiv \langle\langle X\rangle\rangle - X$ is the discrete isotropized laplacian of X. Here we follow the prescription of Ref. [24] for simplifying the short-range terms. In the case of symmetric DBCP, we choose

$$\Gamma(\vec{r},t) = f[\psi(\vec{r},t)] + \mathcal{D}\tilde{\Delta}\psi(\vec{r},t) - b\tilde{\Delta}^2\psi(\vec{r},t), \tag{2}$$

with

$$f(\psi) = (1+\tau)\psi - \tau\psi^3. \tag{3}$$

The first contribution to Γ represents attractive A-A and B-B interactions that lead to segregation of blocks A and B of the DBCPs, since f is a mapping with a flow to two symmetric stable points (it may be derived from a ψ^4 approximation of a free-energy functional). The second term in Eq. 2 is related to local diffusive dynamics and the third one accounts for

the curvature energy of the AB interface. For a review on the model and results, see Ref. [13].

CDM is a simplification of the physico-chemical processes of coarsening systems: the interaction terms have a simple form just to push ψ to the stable points, the same diffusion coefficient is assumed for all chain configurations etc. Thus, it represents universal scaling properties of DBCP domain separation, particularly those morphological properties measured on lengthscales near and above the lamellar size, but CDM is not expected to predict reasonable values of microscopic quantities such as local chain densities.

Most works assume that ψ is a difference of volume fractions of A and B ($\phi_A - \phi_B$) in a cell. However, this assumption makes typical CDM results inconsistent with properties of strongly segregated DBCPs (SSDBCPs). For instance, Fig. 1a shows the ψ profile obtained from CDM using typical parameters of the literature [12, 13, 24]. It is clear that $|\psi|$ is well below 1 in the middle of some domains (see also Ref. [24]). Instead, SSDBCPs have large regions with 100% A or 100% B separated by narrow interfaces, thus $|\phi_A - \phi_B| = 1$ in the middle of those domains. One idea to overcome this problem is to work with parameter ranges corresponding to much lower temperatures, e. g. large values of τ (see Refs. [24, 25]). However, this produces frozen configurations with very small domains (nearly the cell size) for extremely long times.

On the other hand, the pattern morphology of real SSDBCPs is well represented by separating domains of positive and negative ψ in CDM lattices shown in the literature - e. g. compare images in Refs. [1, 26] and CDM patterns in Refs. [12, 13, 24]. This feature and the universality character of CDM (i. e. the fact that CDM always includes the basic physico-chemical mechanisms of the coarsening process of SSDBCPs) lead us to propose a different interpretation of the field variable: (i) the sign of ψ represents the type of chain in a cell, positive for A and negative for B; (ii) the absolute value of ψ is related to the local density at the cell and characterizes a certain position across the domain (ψ may be a non-monotonic function of the local density, to be defined for a specific application); (iii) a range of small values of $|\psi|$ (as defined below) characterizes interfacial and/or mixed regions.

The NPs are assumed to occupy approximately the whole volume of a cell. The state ψ of the CDM cell containing a NP represents neighboring chains interacting with it, i. e. the NP environment. The NP surface chemistry and this environment are responsible for the creation of energy barriers for the NP to move [11, 27]. The NP diffusion is assumed

to take place in nearly equilibrium conditions with the local environment: the higher the barrier, the lower the NP mobility, which indicates a more stable configuration for NP localization. Thus, a NP at position $\vec{r}$ executes random walks among neighboring cells with a diffusion coefficient $D\left[\psi\left(\vec{r},t\right)\right]$, i. e. the rate with which the NP moves to neighboring cells is determined only by the chain configuration at the cell it moved from (and, of course, by the NP properties). Target cells for the NP steps are randomly chosen among the nearest neighbors. Particle-particle interaction is restricted to the excluded volume condition.

However, the presence of a NP in a cell also affects the states of neighboring chains. It is expected that those states evolve not only according to the basic (symmetric) CDM mechanisms, but also that neighboring chains move towards a certain configuration ψ_P that best wets the NP. For this reason, at each time step the state of the NP cell is replaced by

$$\psi_{NP}\left(t+1\right)=\left\langle\left\langle\psi\right\rangle\right\rangle+q\left(\psi_P-\left\langle\left\langle\psi\right\rangle\right\rangle\right), \tag{4}$$

where the first term represents the current neighborhood of the NP and the second one plus the CDM rules represent biased chain diffusion towards the state ψ_P. In this context, q measures the bias intensity. Following this reasoning, the states of NN and next NN (NNN) cells change as

$$\psi_{NN}\rightarrow\psi_{NN}+q/6\left(\psi_P-\psi_{NN}\right) \tag{5}$$

and

$$\psi_{NNN}\rightarrow\psi_{NNN}+q/12\left(\psi_P-\psi_{NNN}\right), \tag{6}$$

respectively (conservation is ensured by suitable changes in their neighborhood).

Although the parameters D, q and ψ_P were interpreted separately, they are related to the same microscopic NP-DBCP interaction, which is determined by DBCP properties and surface chemistry of NPs. For a given application, those parameters cannot be viewed as independent variables. However, the diversity of possible interactions in different systems and the difficulty to predict the real interaction terms suggest to explore them as independent for qualitative applications (in cases of solvent annealing, those parameters may also represent interactions with the solvent). For comparison we recall that previous CDM/NP models assumed that NPs were permanently embedded in a $\psi=1$ shell and had constant diffusion coefficient [14, 15], thus showing the extension of the present approach.

Our simulations were done in square lattices, so that relatively large systems could be simulated up to long times with a reasonable computational effort (this is necessary due to

the large number of parameters to control). A disordered configuration at $t = 0$ is represented by random distributions of ψ in the range $[-0.025, 0.025]$. In some cases we used periodic boundaries, but a large fraction of our simulations use a fixed boundary condition (FBC), where the row $y = 0$ always has $\psi = 1$, in order to represent a material preferentially wet by block A.

A suitable set of CDM parameters (without NPs) were chosen to give the typical ψ profile shown in Fig. 1b after a domain separation time of order $\tau_{SEP} \sim 10^5$. This large value of τ_{SEP} is interesting because it allows the study of the interplay between time scales of different processes. In Fig. 1b, the cells closest to the A-B interface have $-0.1 \leq \psi \leq 0.1$, thus this interval is associated to interfacial and/or mixed regions. The middle of A and B domains are characterized by $|\psi| \approx 0.3 - 0.4$ and the lamellar width is $\lambda \approx 10$. The domain separation pattern obtained under these conditions, shown in Fig. 1c, is similar to those presented in the literature, typically obtained with the parameters of Fig. 1a.

Five simple models for $D(\psi)$ are used to investigate effects of NP mobility.

Letting D_A, D_B, and D_I stand for A, B, and interfacial regions, respectively, the first three models are illustrated in Fig. 2a and defined as: DM1, with $D_B = \frac{1}{2}$, $D_I = \frac{1}{4}$, $D_A = \frac{1}{8}$; DM2, with $D_B = \frac{1}{2}$, $D_I = \frac{1}{20}$, $D_A = \frac{1}{200}$; DM3, with $D_B = \frac{1}{20}$, $D_I = \frac{1}{200}$, $D_A = \frac{1}{20000}$ (these values are given in time and length units of CDM defined above). DM1 represents large mobility in both domains, while DM2 and DM3 have $D_B/D_A \sim 10^2 - 10^3$ [as a rough guide, these are the ratios for Ag NPs in the domains of poly(styrene-b-methylmethacrylate) (PS-PMMA) of Ref. [11]]. This form of $D(\psi)$ is useful to test the effect of different particle mobilities in different domains independently of possible intra-domain variations of $D(\psi)$. With these models, any value $\psi_P \geq 0.1$ is reasonable for representing the effects of NPs on the chains because NP mobility is uniformly low in the whole A domain, where $\psi \geq 0.1$.

Fig. 2b shows the other two diffusion models, where $D(\psi)$ is significantly reduced in certain chain environments, simulating deep energy valleys for NP diffusion at those positions. For consistently describing particle-polymer interaction, the preference of the NP for a certain state [minimum of $D(\psi)$] must be accompanied by a flux of the neighboring chains towards that state. Thus, models DM4 and DM5 are respectively accompanied by $\psi_P = 0.35$ (middle of the A domains - see Fig. 1b) and $\psi_P = 0.1$ (A side of the interfaces).

III. NON-EQUILIBRIUM SELF-ASSEMBLY OF THE COMPOSITE

First we consider the effects of NP mobility on the global alignment of the composites with the FBC.

In Fig. 3a, we show a FBC configuration without NPs obtained at $t = 10^6$, which has ψ profiles similar to Fig. 1b except very close to $y = 0$. In Figs. 3b-d we show FBC configurations at the same time with 0.4% of NPs and diffusion models DM1, DM2 and DM3, respectively. The effect of NPs on the DBCPs is strong in this case, i. e. q is large. It is clearly observed that these small NP concentrations can slow down domain separation or eventually suppress the ordering.

The quality of the alignment with the $y = 0$ border is characterized by the correlation function along the y direction,

$$C_y(y,t) \equiv \langle \psi\left(x',y',t\right) \psi\left(x',y'+y,t\right)\rangle / \langle \left[\psi\left(x',y',t\right)\right]^2 \rangle, \tag{7}$$

with the average taken over x', y' and various realizations. The linear fits of the maxima of $\log|C_y(y,t)| \times y$ plots give the corresponding correlation lengths L_y. Fig 4a shows the time evolution of L_y in the same conditions of Fig. 3a-d. Increasing L_y indicates better alignment of the DBCP lamelles with the interacting border, i. e. a faster global organization of the composite. From Fig. 4a, it is clear that the best alignment with NPs is obtained with diffusion model DM2, followed by DM3 and DM1.

In order to understand these features, an useful quantity is the diffusion length of NPs inside block A at a certain time t, which is given by

$$l_D = (D_A t)^{1/2}. \tag{8}$$

It measures the typical distance swept by a NP after that time if it is confined to the A domain, where it has the lowest mobility.

For DM1, L_y seems to saturate at long times (Fig. 4a), indicating that only a finite region near the bottom surface is aligned, while the rest of the sample is disordered. Simulation without the aligning surface provides a completely disordered lattice, i. e. there is no phase separation even at long times. $\psi_P = 0.35$ and $q = 0.1$ were used in those simulations, so that the A chains are rapidly pulled to the NP neighborhood, but the fast movement of the NPs do not allow the chains to reorganize around them. Indeed, at the separation time

τ_{SEP} of the pure system, we have $l_D \approx 112$, which is much larger than the lamellar size λ and explains the disordering effect of NPs. These NPs are equivalent to a thermal noise that brings the system above an order-disorder transition (ODT). It parallels the finding of Ref. [16] that the ODT temperature of poly(styrene-b-isoprene) (PS-PI) decreases as the concentration of mixed silica particles increases.

On the other hand, very small mobility (DM3) does not disturb phase separation in the middle of the lattice, as shown in Fig. 3d. Indeed, fixed NPs may improve local organization, as discussed in Ref. [28]. However, they slow down the alignment with the border $y = 0$ because they may freeze a local order which does not match the order near the bottom surface. The slowly increasing global ordering is confirmed by the slow increase in L_y of Fig. 4a. The NP diffusion length inside the A domain at τ_{SEP} is $l_D \approx 2$, while $l_D \approx 7$ at $t = 10^6$ (Fig. 2d). These values of l_D are both smaller than the lamellar width $\lambda \approx 10$, justifying the interpretation of these slow particles as pinning centers of a local domain configuration. The internal domain separation much faster than the global ordering of the sample was experimentally observed in composites of poly(styrene-b-2-vinylpyridine) (PS-P2VP) and $CdSe$ particles [17].

The fastest global ordering (largest L_y) is obtained with DM2, where NPs in block A have $l_D \approx 22$ at τ_{SEP}. This value of l_D is near the domain period 2λ, thus NPs can solidarily move with the neighboring chains to the most favorable positions without generating undesired noise. Other values of q and ψ_P lead to the same result. Thus, matching NP diffusion length and lamellar period at the pure DBCP ordering time τ_{SEP} may reduce the organization time τ_C of the composite with the same morphology. In general, increasing temperature increases D and τ_{SEP}, thus it also increases l_D (but may decrease τ_C by bringing it closer to τ_{SEP}). This may be crucial for technological applications where the experimental separation times upon annealing are several hours or days.

As expected, the effect of increasing NP concentration is to increase the time for global alignment, or reduce L_y at a fixed time. This is shown in Fig. 4b for diffusion model DM3 (very small NP mobility). It parallels the increase of the characteristic time for lamellar alignment of PS-PMMA films with Ag particles reported in Ref. [23].

In Figs. 4a and 4b, we note that L_y scales diffusively with time (i. e. as $t^{1/2}$) in the pure DBCP, but the presence of NPs seems to lead to slower coarsening. It is not clear for us if there is a change in the universality class of this non-equilibrium system due to the NPs or

if this is a consequence of corrections to the main scaling form. This may be an interesting point for future theoretical investigation, but certainly much more accurate data in larger system sizes would be necessary.

IV. MORPHOLOGICAL CHANGES

The increase of NP concentration also has drastic effects on the composite patterns at long times. The steady states of the CDM/NP model are able to represent experimental features of some composites in thermodynamic equilibrium.

First we analyze the effect of NP concentration with no aligning border. Configurations at $t = 10^6$ are shown in Figs. 5a-c, respectively without NP and with 0.8% and 3.2% of NPs. The pure DBCP has highly parallel lamellae (Fig. 5a) and this structure has only small deformation with low NP concentration (Fig. 5b). However, it changes to a hexagonal structure with 3.2% of NPs (Fig. 5c), even with weak effects of the NPs on the chains ($q = 0.02$). This is not a lattice effect because the CDM used square grids. This is a morphological transition caused by the stretching of the A domains that wet moving NPs, and can be achieved with smaller concentrations for larger values of q.

Such transitions were experimentally observed in Ref. [20] with PS-covered Au particles in PS-P2VP. In Ref. [21], metallic and magnetic NPs changed the morphology of PS-PI from cylindrical to spherical domains; the two-dimensional projections of those patterns correspond to the lamellar-hexagonal transition illustrated in Figs. 5a-c (see Fig. 2 of Ref. [21]). Refs. [20] and [22] show the opposite transition, from hexagonal to lamellar morphology, but these are also cases where NPs stretched one of the domains. Finally, the hexagonal morphology of PS-P2VP films was preserved with high loadings of $CdSe$ particles in Ref. [29], which suggests that suitable NP coatings were able to reduce NP effects on the chains.

Even before these experiments were performed, NP-induced morphological transitions were theoretically predicted using different thermodynamic equilibrium models, e. g. in Refs. [8, 9, 20, 30]. The stretching of A domains by NPs was already shown in previous CDM/NP models [14, 15], but no morphological transition was reported there. A recent work with dissipative particle dynamics (DPD) [31] only showed deformation of the lamellar structure of DBCP with NPs. Thus, the novelty of the present approach is to show how

those transitions arise from a non-equilibrium cooperative dynamics.

The increase of NP loading may also lead to the coexistence of different patterns in a single sample in contact with an aligning surface (FBC). This is shown in Figs. 6a and 6b, where the samples have parallel lamellae near the surface and nearly hexagonal order far from it. The increase of NP concentration and the preferential location near the interfaces (i. e. $\psi_P \approx 0.1$) favor the formation of the hexagonal structure, since the NPs have larger diffusion lengths near the interfaces and more easily stretch them. The concentration to obtain the coexisting patterns may vary, but a minimum cooperative effort of the set of NPs (high q or high concentration) is required to produce it. Similar structures were not shown in previous theoretical work, but it is interesting to recall that Ref. [32] showed evidence that non-selective NPs (which tend to go to the interfaces) favor morphological transitions from a lamellar phase, as illustrated here.

Different patterns in a single sample were already observed experimentally. Thick films of PS-P2VP containing PS-covered Au particles [5] showed a lamellar structure near the air-polymer interface and a cylindrical structure (cross section with hexagonal packing) near the substrate. The lamellar region propagated to longer distances compared to Figs. 6a-b, possibly affected by solvent evaporation and reduction of local NP concentration - similar effects of solvent concentration were reported in Ref. [33]. Moreover, in Ref. [23], different patterns in a single sample were clearly observed: large Ag particles froze lamellar configurations of PS-PMMA perpendicular to the aligning (but relatively distant) substrate. The particular NP location in that case was related to the interaction with the air interface, but the overall effect of NPs with low mobility is similar to that in Fig. 3d.

V. NP DISTRIBUTIONS ACROSS ALIGNED DOMAINS

The NP position distributions across the parallel lamellae (FBC) can be also related to NP diffusion.

If the NP diffusion coefficient is not very different in A and B domains (model DM1), then large fractions of NPs are found in the B domains. For instance, for low values of q (e. g. $q = 0.02$), a parallel lamellar organization is obtained with more than 10% of NPs in the B domains.

However, a significant localization of the NP inside the A domains is obtained for models

DM2 and DM3, where the mobility in the A domains is much smaller than in the B domains. In Fig. 7a, we show long time probability densities $P(y)$ of finding a NP at position y (measured relatively to the center of a lamellae) for DM2 with different values of ψ_P. In both cases the NPs are distributed almost uniformly inside the A domains, with sharp concentration decrease at the interfaces. Usually less than 1% of the NPs are in the B domain and less than 15% in the interfacial region.

Similar shapes of $P(y)$ are found for a broad range of parameters q and ψ_P and models DM2 and DM3. Thus, if the overall effect of surface chemistry and polymer properties is to reduce NP mobility across the whole A domain, then the NP distribution is broad, independently of the chain configuration that tends to move to the NP neighborhood. In these cases, the adjustments in chain configuration around the NPs (bias towards the state ψ_P) are balanced out by thermal effects, while slow NP movement avoids undesirable noise.

On the other hand, highly peaked $P(y)$ are obtained with DM4 and DM5, as shown in Fig. 7b. These are the cases where the NPs have severely reduced mobility in a certain position of the A domains [minimum of $D(\psi)$ - Fig. 2b]. This position determines the preferential localization of NPs: the center of the A domains for DM4 and the interfaces for DM5.

These results suggest that the localization of NPs strongly depends on the surface chemistry being able to provide a favorable interaction with a particular chain configuration, which may be the middle of the A domains or the interface in the above examples. This favorable interaction corresponds to some energy valley at that position, which reduces NP diffusion coefficient. Of course additional conditions are important for the global organization, such as reduced NP effects on the chains and avoidance of pinning effects due to very low NP mobility, as discussed in Sec. III.

The above NP distributions resemble those of Kim et al [18, 19] for Au particles in thick films of PS-*b*-P2VP: preferential localization of the NPs in the center of the PS lamellae or at the interface with P2VP, depending on the density of coatings (PS or P2VP) of the NP surface. Recently, the same group [34] showed NP position distributions similar to those in Figs. 7a-b using various coatings. This suggests to search for an interpretation based on position-dependent diffusion energy barriers during the annealing process.

VI. SUMMARY AND CONCLUSION

We proposed a cell dynamics model for DBCP domain separation interacting with randomly moving NPs. Increasing NP concentration slows down separation and global alignment, but this effect is reduced by matching the lamellar size and NP diffusion lengths. The model also represents various features of real composites, such as morphological transitions induced by NPs, the coexistence of different patterns in a single sample and various NP density profiles across the lamellae.

Previous works also predicted localized NP distributions [32, 35, 36, 37, 38] and morphological transitions [8, 9, 20] in thermodynamic equilibrium, but an advantage of the CDM/NP approach is to explore the non-equilibrium routes leading to those and other properties. An additional advantage is the low computational cost; for instance, one configuration of a 256×256 lattice at $t = 10^6$ is generated in less than two hours in a desktop. This is important if one aims at testing hypothesis theoretically before performing series of experiments. Quantitative application is possible by associating the time and length scales involved in the domain coarsening (e. g. τ_{SEP} and λ) to experimental values and choosing sensible values of the other parameters. Certainly the model can also be extended, for instance to include in-situ NP formation or NP interaction.

Acknowledgment. The author thanks Robert Hamers, Andrew Mangham and Divya Goel for helpful discussion, acknowledges support from CNPq for his visit to UW and acknowledges support from CNPq and Faperj (Brazilian agencies) for his simulation laboratory at UFF, Brazil.

---

[1] Hamley, I. W. *Nanotechnology* **2003**, 14, R39.

[2] Bockstaller, M. R.; Mickiewicz, R. A.; Thomas, E. L. *Adv. Mater.* **2005**, 17, 1331.

[3] Lin, Y.; Böker, A.; He, J.; Sill, K.; Xiang, H.; Abetz, C.; Li, X.; Wang, J.; Emrick, T.; Long, S.; Wang, Q.; Balazs, A.; Russel, T. P. *Nature* **2005**, 434, 55.

[4] R. B. Grubbs, J. Polym. Sci. Part A: Polym. Chem. **43**, 4323 (2005).

[5] Kim, B. J.; Chiu, J. J.; Yi, G.-R.; Pine, D. J.; Kramer, E. J. *Adv. Mater.* **2005**, 17, 2618.

[6] Balazs, A. C.; Emrick, T.; Russel, T. P. *Science* **2006**, 314, 1107.

[7] Warren, S. C.; Disalvo, F. J.; Wiesner, U. *Nature Mater.* **2007**, 6, 156.

[8] Thompson, R. B.; Ginzburg, V. V.; Matsen, M. W.; Balazs, A. C. *Science* **2001**, 292, 2469.

[9] Lee, J. Y.; Thompson, R. B.; Jasnow, D.; Balazs, A. C. *Macromolecules* **2002**, 35, 4855.

[10] Zeng, Q. H.; Yu, A. B.; Lu, G. Q. *Prog. Polym. Sci.* **2008**, 33, 191.

[11] Lopes, W. A.; Jaeger, H. M. *Nature* **2001**, 414, 735.

[12] Oono, Y.; Bahiana, M. *Phys. Rev. Lett.* **1988**, 61, 1109; Bahiana, M.; Oono, Y. *Phys. Rev. A* **1990**, 41, 6763.

[13] Hamley, I. W. *Macromol. Theory Simul.* **2000**, 9, 363.

[14] Balazs, A. C.; Ginzburg, V. V.; Qiu, F.; Peng, G.; Jasnow, D. *J. Phys. Chem. B* **2000**, 104, 3411.

[15] Ginzburg , V. V.; Gibbons, C.; Qiu, F.; Peng, G.; Balazs, A. C. *Macromolecules* **2000**, 33, 6140.

[16] Jain, A.; Gutmann, J. S.; Garcia, C. B. W.; Zhang, Y.; Tate, M. W.; Gruner, S. M.; Wiesner, U. *Macromolecules* **2002**, 35, 4862.

[17] He, J.; Tangirala, R.; Emrick, T.; Russel, T. P.; Böker, A.; Li, X.; Wang, J. *Adv. Mater.* **2007**, 19, 381.

[18] Chiu, J. J.; Kim, B. J.; Kramer, E. J.; Pine, D. J. *J. Am. Chem. Soc.* **2005**, 127, 5036.

[19] Kim, B. J.; Bang, J.; Hawker, C. J.; Kramer, E. J. *Macromolecules* **2006**, 39, 4108.

[20] Sides, S. W.; Kim, B. J.; Kramer, E. J.; Fredrickson, G. H. *Phys. Rev. Lett.* **2006**, 96, 250601.

[21] Park, M. J.; Park, J.; Hyeon, T.; Char, K. *J. Pol. Sci.* **2006**, 44, 3571.

[22] Yeh, S.-W.; Wei, K.-W.; Sun, Y.-S.; Jeng, U-S.; Liang, K.-S. *Macromolecules* **2005**, 38, 6559.

[23] Deshmukh, R. D.; Buxton, G. A.; Clarke, N.; Composto, R. J. *Macromolecules* **2007**, 40, 6316.

[24] Ren, S. R.; Hamley, I. W. *Macromolecules* **2001**, 34, 116.

[25] Ohta, T; Kawasaki, K. *Macromolecules* **1986**, 19, 2621.

[26] Darling, S. B. *Prog. Polym. Sci.* **2007**, 32, 1152.

[27] Gopinathan, A. *Phys. Rev. E* **2005**, 71, 041601.

[28] Lee, B. P.; Douglas, J. F.; Glotzer, S. C. *Phys Rev E* **1999**, 60, 5812.

[29] Zou, S.; Hong, R.; Emrick, T.; Walker, G. C. *Langmuir* **2007**, 23, 1612.

[30] Huh, J.; Ginzburg, V. V.; Balazs, A. C. *Macromolecules* **2000**, 33, 8085.

[31] He, L.; Zhang, L.; Liang, H. *J. Phys. Chem. B* **2008**, 112, 4194.

[32] Pryamitsyn, V.; Ganesan, V. *Macromolecules* **2006**, 39, 8499.

[33] Deshmukh, R. D.; Liu, Y.; Composto, R. J. *Nano Lett.* **2007**, 7, 3662.

[34] Kim, B. J.; Fredrickson, G. H.; Kramer, E. J. *Macromolecules* **2008**, 41, 436.

[35] Liu, D.; Zhong, C. *Macromol. Rapid. Commun.* **2006**, 27, 458.

[36] Jin, J.; Wu, J. *J. Chem. Phys.* **2008**, 128, 074901.

[37] Matsen, M. W.; Thompson, R. B. *Macromolecules* **2008**, 41, 1853.

[38] Kang, H.; Detcheverry, F. A.; Mangham, A. N.; Stoykovich, M. P.; Daoulas, K. C.; Hamers, R. J.; Müller, M.; de Pablo, J.; Nealey, P. F. *Phys. Rev. Lett.* **2008**, 100, 148303.

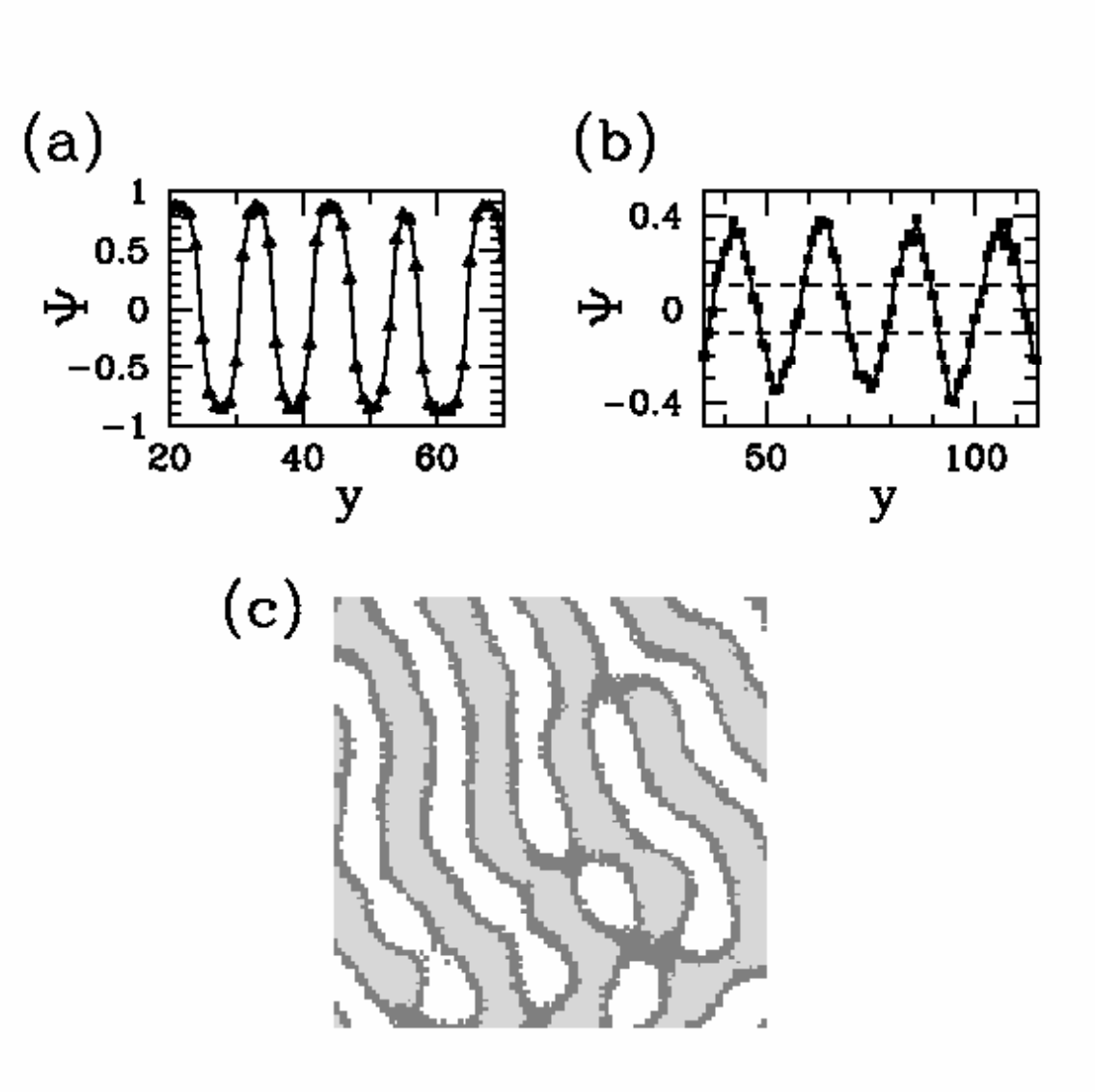

FIG. 1: (a) Long time ψ profiles in directions perpendicular to the parallel DBCP domains without NPs and traditional parameters of the literature: $\tau = 0.3$, $D = 0.5$, $B = 0.005$, $b = C = 0$. (b) Profiles with typical parameters of this work: $\tau = 0.035$, $D = 0.5$, $B = 0.0005$, $b = 0.35$, $C = 0.02$; the region between dashed lines is the interfacial and/or mixed region. (c) Typical lattice configuration at $\tau_{SEP} = 10^5$ obtained with the CDM parameters of this work. A (B) domains are light gray (white) and interfacial regions are medium gray.

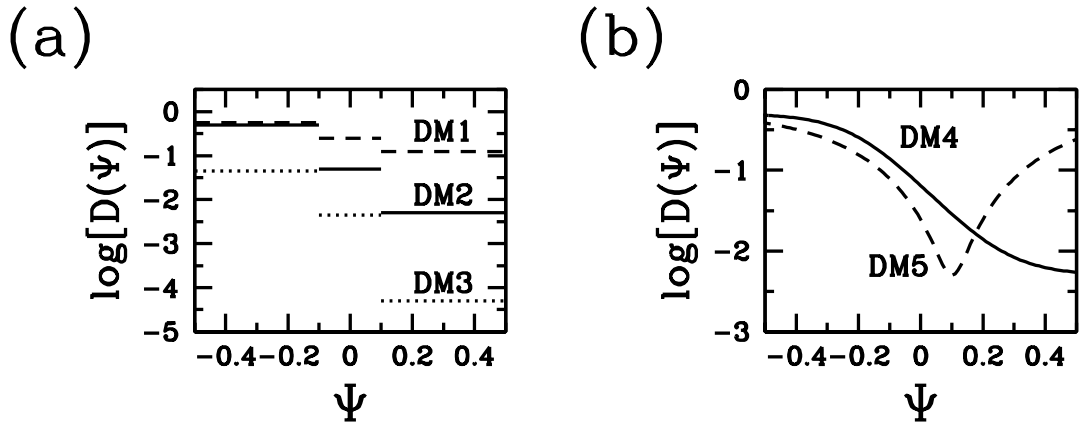

FIG. 2: Diffusion models: (a) DM1 (dashed lines), DM2 (solid lines), and DM3 (dotted lines); (b) DM4 (solid line) and DM5 (dashed line).

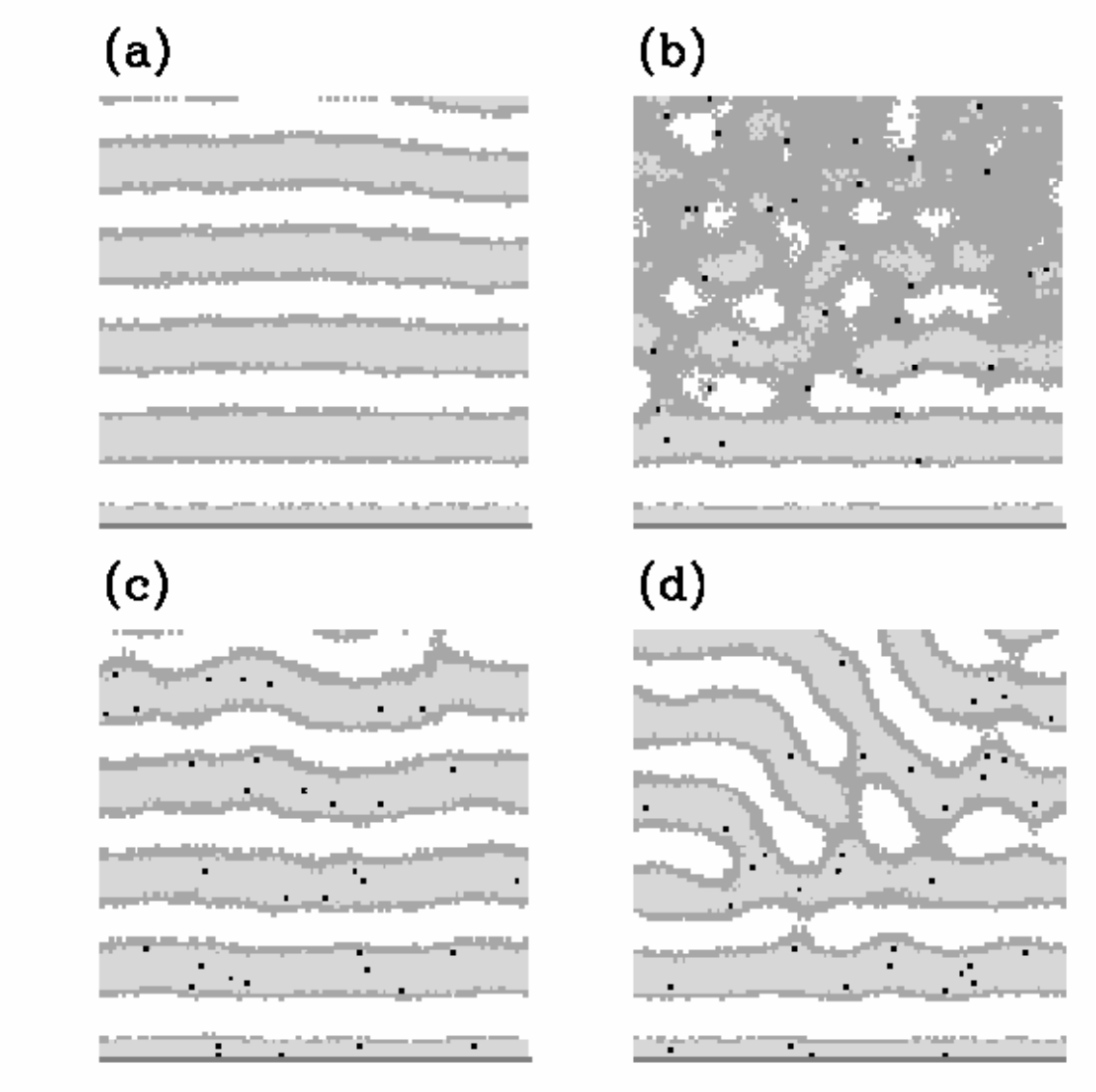

FIG. 3: Typical lattice configurations at $t = 10^6$ with the FBC: a) without particles; b), c), d) 0.4% of NPs with DM1, DM2 and DM3, respectively, $q = 0.1$, and $\psi_P = 0.3$. Surface with fixed $\psi = 1$ is dark gray, A (B) domains are light gray (white), interfacial regions are medium gray, and NPs are black.

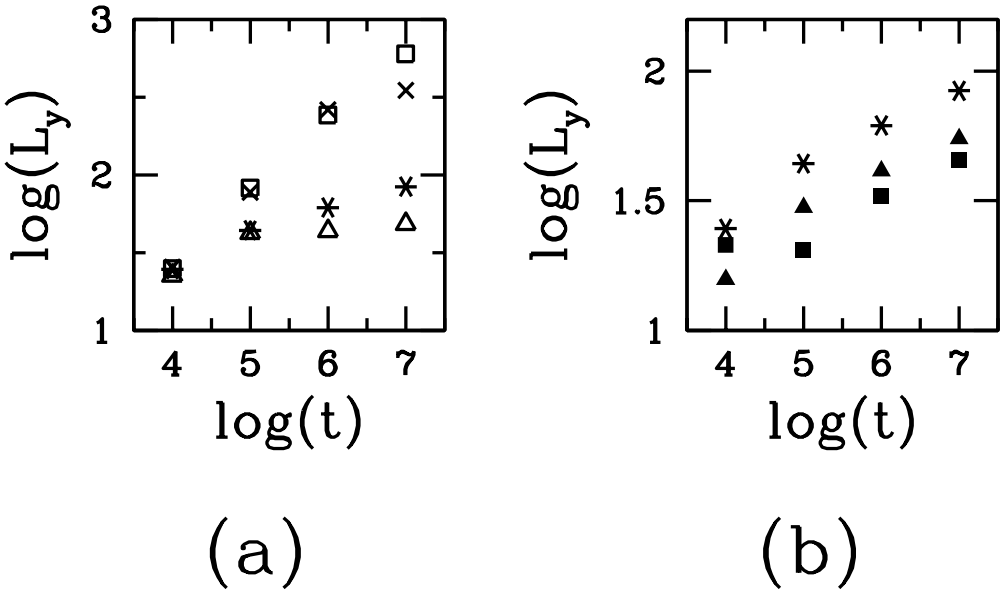

FIG. 4: Time evolution of correlation length with the FBC: (a) same conditions of Fig. 2, with no particles (squares), DM1 (triangles), DM2 (crosses), and DM3 (asterisks); (b) diffusion model DM3 with the same q and ψ_P of Fig. 2, and NP concentrations 0.4% (asterisks), 0.8% (filled triangles), and 1.6% (filled squares). Error bars are near the size of the points.

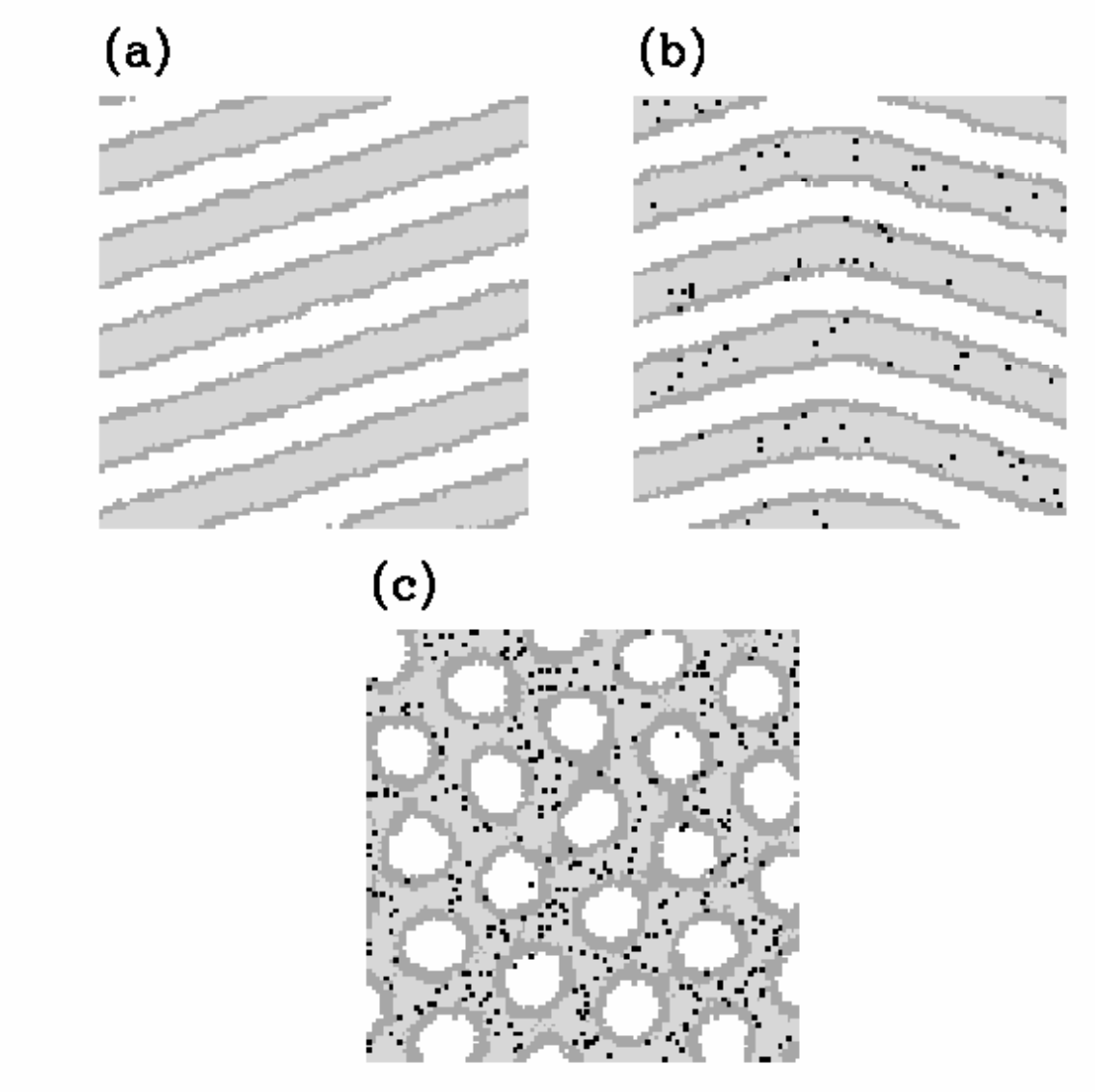

FIG. 5: Typical lattice configurations at $t = 10^6$ without (a), with 0.8% (b) and with 3.2% (c) of DM2 NPs, no aligning boundary, $b = 0.05$, $q = 0.02$, and $\psi_P = 0.3$. Color scheme is the same of Fig. 2.

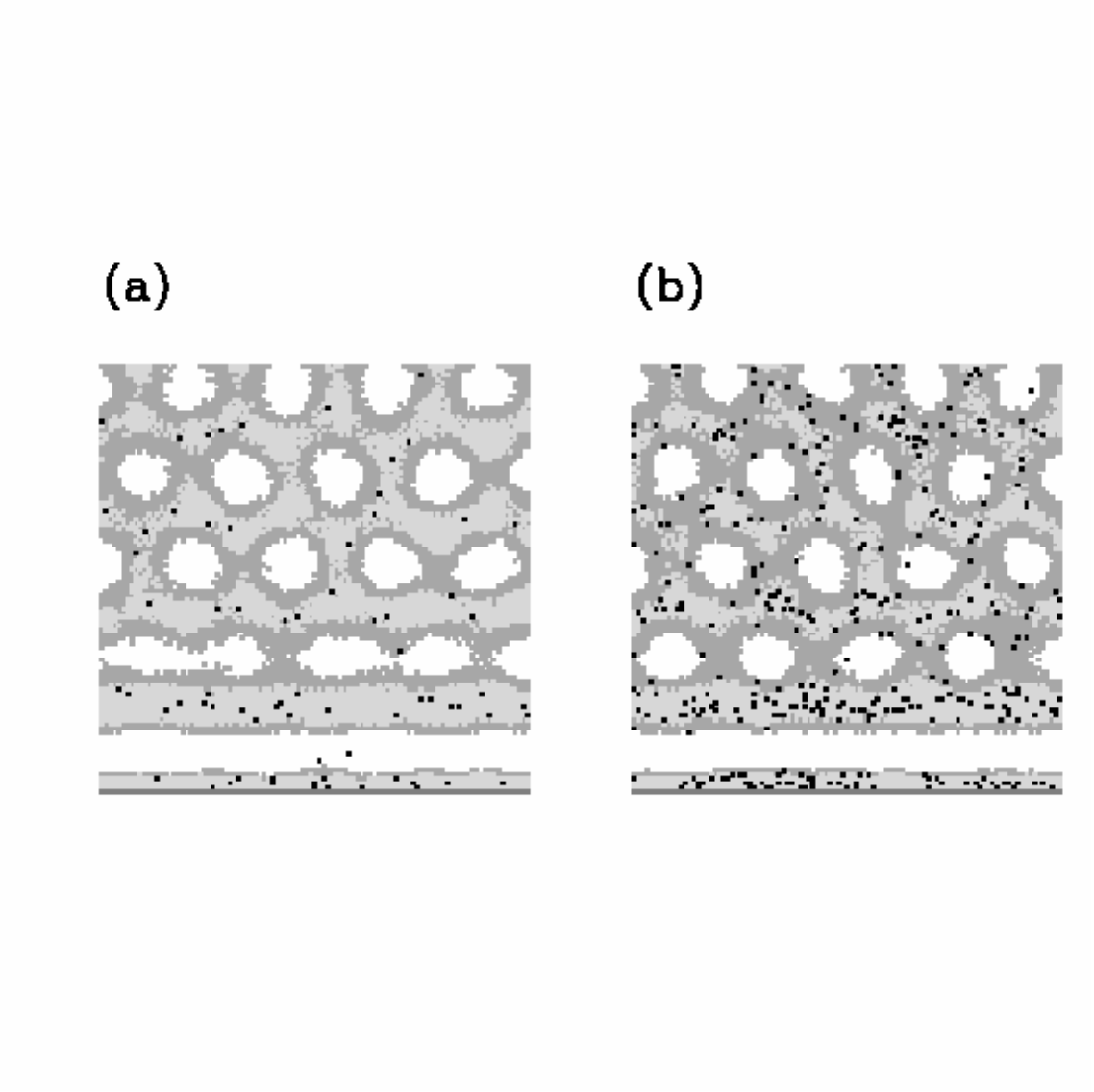

FIG. 6: Typical lattice configurations with FBC at $t = 10^7$ and: (a) 0.8% of DM2 NPs, $b = 0.35$, $q = 0.1$, and $\psi_P = 0.1$; (d) 3.2% of DM5 NPs, $b = 0.35$, $q = 0.02$, and $\psi_P = 0.1$. Color scheme is the same of Fig. 2.

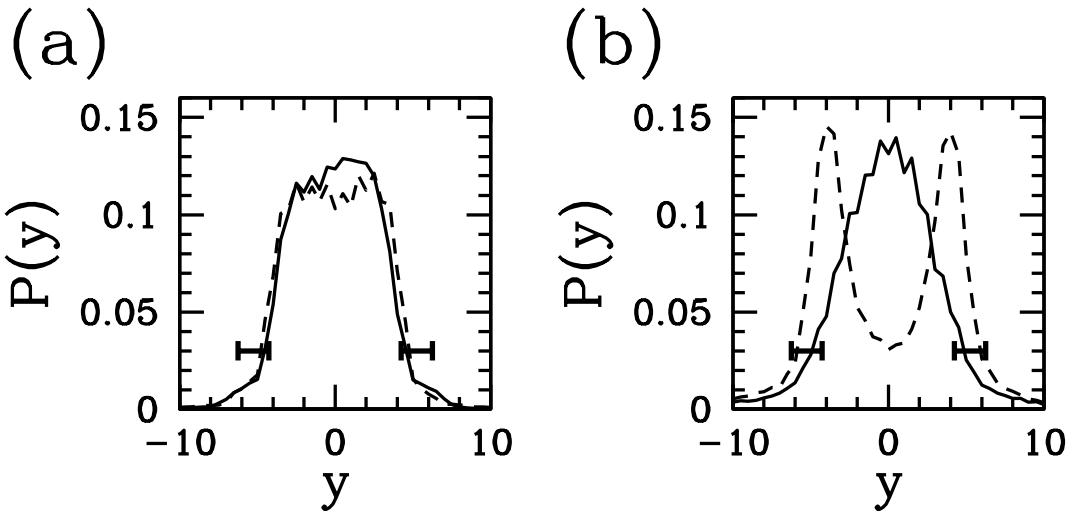

FIG. 7: NP position distributions across the parallel lamellae for: (a) DM2 with $\psi_P = 0.1$ (solid line) and $\psi_P = 0.35$ (dashed line); (b) DM4 with $\psi_P = 0.35$ (solid line) and DM5 with $\psi_P = 0.1$ (dashed line). Horizontal bars indicate typical interface regions.